Simulating the Poisson effect in lattice models of elastic continua

Author links open overlay panel D.Asahina[a] K.Ito[a] J.E.Houseworth[b] J.T.Birkholzer[b] J.E.Bolander[c]

[a]National Institute of Advanced Industrial Science and Technology (AIST), Higashi 1-1-1, Central 7, Tsukuba, Ibaraki 305-8567, Japan

[b]Earth Sciences Division, Lawrence Berkeley National Laboratory, One Cyclotron Rd, Berkeley, CA 94720, USA

[c]Department of Civil and Environmental Engineering, University of California, Davis, One Shields Avenue, Davis, CA 95616, USA

Available online 8 August 2015

https://doi.org/10.1016/j.compgeo.2015.07.013

Lattice models provide discontinuous approximations of the displacement field over the computational domain, which facilitates the modeling of fracture and other discontinuous phenomena. By discretizing the domain with two-node elements, however, ordinary lattice models cannot simulate the Poisson effect in a local (intra-element) sense, which is problematic for some types of analyses. Furthermore, such methods are limited in the range of Poisson ratio values that can be simulated. We present a new approach to remedy such known, yet underappreciated, shortcomings of lattice models. In this approach, the Poisson effect is modeled through the introduction of fictitious stresses into a regular lattice. Capabilities of the new approach are demonstrated through compressive test simulations of homogeneous and heterogeneous materials. The simulation results are compared with theory and those of continuum finite element models. The comparisons show good agreement for arbitrary Poisson ratios (including $\nu \geqslant 1/3$) with respect to nodal displacement, intra-element stress, and nodal stress. This form of discrete method, supplemented by the proposed fictitious measures of stress, retains the simplicity of collections of two-node elements.

1. Introduction

Lattice models are attractive for simulating the fracturing of various materials, particularly when fracture development is affected by material structure or other forms of heterogeneity present at the scale of discretization. Lattice models are typically based on a set of nodes and their interconnection via primitive, one-dimensional (1-D) elements. Such models, which include some types of particle models, can be viewed as mechanical analogues of the equations of continuum mechanics [1], [16], [21], [31]. The nodes can be arranged in regular or irregular patterns. Continuum properties are obtained, in an approximate sense, through appropriate assignments of the element properties. As described herein, however, lattice models are limited in their abilities to represent local stress conditions, particularly with respect to the influence of Poisson's ratio [6], [18], [12]. Proper representation of the Poisson effect is an essential ingredient within most rock mechanics simulations, including those affected by multiaxial stress conditions or material heterogeneity. Beginning with the work of Hrennikoff [19], a variety of discrete methods have been developed to represent continua as collections of particles or lattice structures. Particle-based methods, including the discrete element method [9], are used to simulate the interaction of discrete features and their collective influence on the behavior of geological systems. Micro-mechanical parameters used in the discrete elements (i.e., springs or bonds between the particles) can be determined, through calibration with laboratory results, to represent macroscopic material behavior [38]. Random particle

models are also used to simulate fracture behavior of other geomaterials such as concrete [4], [10]. Macroscopic representation of the Poisson effect is accomplished by adjusting the ratio of the average strain between the longitudinal and transverse directions [10], [11]. Lattice models are another means for studying elasticity and breakdown of a variety of materials and structures [17], [33], [22], [15]. Global representation of Young's modulus and Poisson's ratio can be obtained by adjusting longitudinal and transverse dimensions, or stiffnesses, of the lattice beam elements [8], [3], [36]. Whereas such models simulate the Poisson ratio in a global sense, inaccuracies are present at the elemental level, which can be viewed as an artificial form of heterogeneity that is not present in most models constructed from continuum elements. Moreover, direct linkages between input mechanical parameters and experimental measurements are difficult to establish for discrete methods [31].

The elasticity of discrete methods, without using free parameters, has been studied. Griffiths and Mustoe [16] relate the elastic constants, Young's modulus and Poisson's ratio, and the spring stiffnesses through an approach based on strain energy density. Such relations are used herein for comparison purposes. Liu et al. [25] derive similar relationships to model failure behaviors such as breaking displacement, shear resistance, and coefficient of friction. Alternatively, three-node discrete element models have been developed to accommodate a volumetric constitutive relation. Hori et al. [18] proposed a discrete-type finite element model based on the use of discontinuous shape functions for each node. Cusatis and Schauffert [12]developed an integrated framework between discrete and continuum methods to overcome the disadvantages of discrete methods. A local representation of both Young's modulus and Poisson's ratio was obtained by a hybrid system, in which a planar lattice is combined with constant strain triangle finite elements [6]. Although these discrete approaches accurately represent the Poisson effect with a set of discrete springs, or in conjunction with finite elements, the simplicity of two-node elements (as a means for modeling material breakdown) is compromised. Munjiza [27] developed a combined finite–discrete element method (FDEM), in which elasticity calculations are based on continuum finite element methods, and discontinuous behavior is represented by a discrete method. Whereas the transition from continuous to discontinuous behavior needs proper attention [5], [29], [30], [34], FDEM capably simulates both elasticity and failure processes of geomaterials, as demonstrated through comparisons with theory and laboratory studies [26], [24]. Munjiza et al. [28] cover several methods that describe physical systems using discrete entities.

This paper calls attention to significant shortcomings of discontinuous (lattice) models with respect to simulating stress conditions within elastic continua. In particular, models constructed with discrete, two-node, elements do not provide a local representation of the Poisson effect. Furthermore, such models do not accommodate the full range of Poisson's ratio, nor even the range exhibited by some rocks [14]. A new approach is presented to address these known, yet underappreciated, shortcomings. Transverse strains, based on fictitious measures of principal stress calculated at the nodal points, are iteratively introduced to accurately represent the Poisson effect within a regular lattice. With the proposed approach, element stiffnesses are based directly on the material properties (i.e. Young's modulus and Poisson's ratio), such that calibration processes are not necessary. To

demonstrate the accuracy of the proposed approach, simulation results for homogeneous systems under uniform loading are compared with both analytical solutions and practical relationships, which have been widely used to determine the spring constants of discrete methods. Comparisons are made for intra-element stress, nodal stress, and nodal displacement. Thereafter, the accurate modeling of multi-phase systems is demonstrated through comparisons with finite element results.

2. Modeling of elastic continua: limitations of lattice models

Lattice models are based on discontinuous approximations of the field variable over the computational domain. This facilitates the modeling of fracture development and other discontinuous phenomena. However, there are significant shortcomings of lattice models with respect to representing local stress conditions. For example, for the boundary conditions and loading shown in Fig. 1a, conventional continuum approaches predict uniaxial compressive stress at any point within the domain. All normal stress components are either compressive or have zero magnitude. Lateral straining (i.e., the Poisson effect) occurs, in accordance with theory. Consider a regular truss network, configured as shown in Fig. 1b and likewise loaded in compression. It exhibits lateral straining, but only at a fixed proportion of the vertical compressive strain. Furthermore, the lateral truss elements are in tension, which disagrees with conventional theories of elasticity. Such truss networks exhibit vertical cracking when the lateral tension reaches the prescribed tensile strength of the material. Whereas cracking parallel to the direction of compressive loading has been observed during physical testing, such cracking is typically a consequence of finer-scale material heterogeneity and is more appropriately related to strain capacity. Moreover, the truss element forces depend on the orientation of the truss network with respect to the direction of loading.

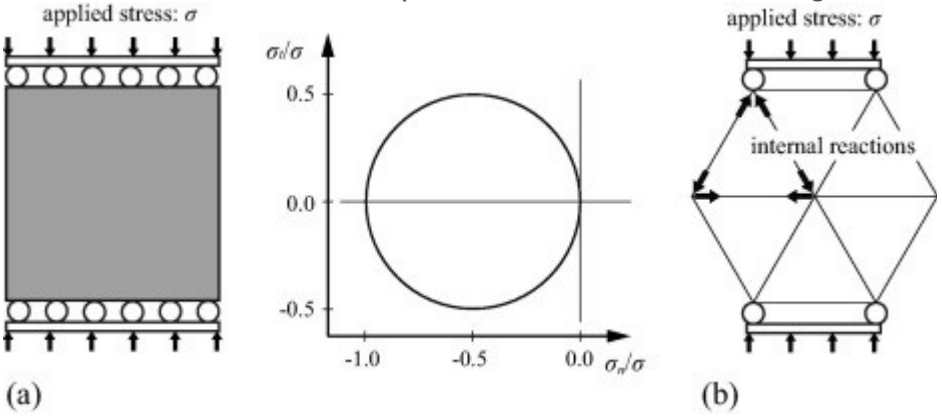

Download high-res image (138KB)

Download full-size image

Fig. 1. Model response to uniaxial compression: (a) homogeneous continuum and Mohr circle representation of the stress state, where σ_n and σ_t represent normal and tangential stress, respectively (tensile stress is positive), and (b) unit cell of a regular network of truss elements.

By supplementing the truss elements with shear and rotational stiffnesses, a range of macroscopic Poisson ratio can be simulated. One such lattice model is presented in the following section. The macroscopic Poisson ratio can be controlled by adjusting the relative magnitudes of the axial and

shear stiffnesses. However, such lattice models provide a flawed representation of the Poisson effect: under uniaxial compressive loading, tension is wrongly produced in the orthogonal direction.

3. Lattice model formulation

Hereafter, a specific form of lattice model, based on the rigid-body-spring concept of Kawai [23], is used to discretely represent elastic continua. This approach has been used to simulate elasticity and breakdown of a variety of materials [7], [13], [2]. For a triangular array of nodal points, the lattice geometry is shown in Fig. 2a. In this study, nodal connectivity is prescribed and remains constant throughout the analysis: contact modeling used in the Distinct Element Method (DEM) is not considered. For this 2-D case, each node has two translational and one rotational degrees of freedom. Each element *ij* is composed of a zero-size spring set that is connected to nodes *i*and *j* via rigid links. The spring set is formed from two axial (normal and tangential) springs, k_n and k_t, and one rotational spring, k_φ, as shown in Fig. 2b. The spring coefficients are assigned according to

$$k_t = \alpha_1 k_n = \alpha_1 \alpha_2 E \frac{A_{ij}}{h_{ij}}, \quad k_\varphi = E \frac{I_{ij}}{h_{ij}} \tag{1}$$

in which E is the Young's modulus, A_{ij} is the area of the facet common to nodes i and j (Fig. 2a), h_{ij} is the distance between the same nodes, and I_{ij} is the second moment of area A_{ij}. By adjusting α_1 and α_2, macroscopic modeling of both elastic constants (E and Poisson ratio, ν) is possible.

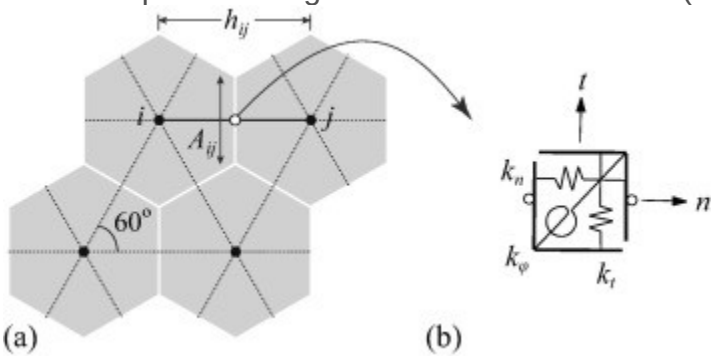

Download high-res image (81KB)

Download full-size image

Fig. 2. (a) Portion of a triangular mesh; and (b) a zero-size spring set located at the centroid of A_{ij} within element *ij*.

By equating strain energy densities of an elastic continuum (in plane stress) and a regular triangular lattice, the spring coefficients are related to the elastic constants as follows [16]:

$$k_n = \frac{E}{\sqrt{3}(1-\nu)}, \quad k_t = \frac{E(1-3\nu)}{\sqrt{3}(1-\nu^2)} \tag{2}$$

where the range of Poisson ratio is limited to $-1 < \nu < 1/3$. Similar formulations can be found elsewhere [20], [25] and are widely used to determine the spring constants of discrete methods. For a particular value of the Poisson ratio, it is possible to rewrite Eq. (2) in terms of α_1 and α_2. For example, for $\nu = 0.2$, α_1 and α_2 become 1.25 and 1.25/3, respectively, which are used herein for comparison purposes. Whereas strain conditions obtained by Eq. (2) for regular lattices have been validated, the

local stress conditions have not been discussed [16]. The following section introduces existing procedures to determine local stress conditions from the lattice structure, and a new approach to accurately represent the Poisson effect.

4. Elastic stress analysis

4.1. Stress calculation

The state of stress can be determined within the lattice elements or at the nodes [32], [37]. After solving the governing field equations to determine nodal displacements, the forces within the normal and tangential springs ($F_n$and F_t) are calculated. These spring forces are used in each of the following forms of stress calculation.

Intra-element stress vector: The stresses associated with the normal and tangential springs are

$$\sigma_n = F_n/A_{ij}, \quad \text{and} \quad \sigma_t = F_t/A_{ij} \tag{3}$$

The rotational spring contributes to the element stiffness, but it is not considered in the stress calculations.

Nodal stress tensor: The hexagonal cell associated with node *i* is sectioned through the node and perpendicular to the direction of interest defined by angle θ (Fig. 3). The forces on the newly formed cut face are determined by summing the weighted force contributions of all *M* elements connecting into the node [6], [37]:

$$F_{n\theta} = \sum_{m=1}^{M} R_m [F_{nm} \cos(\pi - \varphi_m + \theta) + F_{tm} \sin(\varphi_m - \theta)] \tag{4}$$

$$F_{t\theta} = \sum_{m=1}^{M} R_m [F_{nm} \sin(\pi - \varphi_m + \theta) + F_{tm} \cos(\varphi_m - \theta)] \tag{5}$$

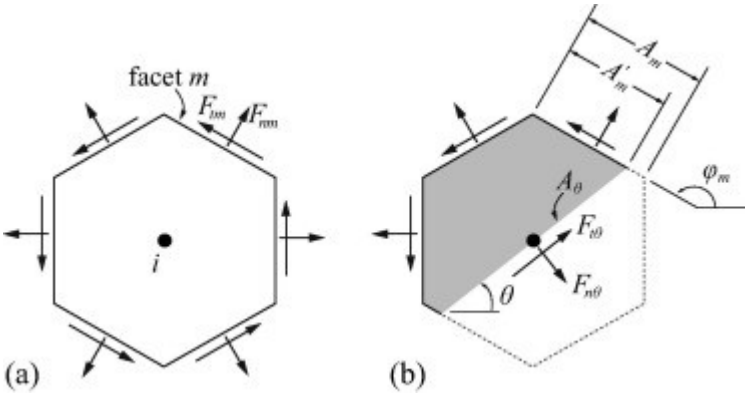

Download high-res image (100KB)

Download full-size image

Fig. 3. (a) Force components acting on each facet of a hexagonal cell, and (b) force components on cut face defined by angle θ.

The weighting factor R_m is set equal to A'_m/A_m, where A_m is the area of facet *m* and A'_m is the area of facet *m* on the negative side of the cut plane, with respect to the normal direction (Fig. 3b). If the cut

plane intersects the facet, $0 < R_m < 1$; otherwise, R_m equals zero or unity depending on whether all vertices of facet m are located on the positive or negative side of the cut plane, respectively. The stress components are then

$$\sigma_{n\theta} = F_{n\theta}/A_\theta, \quad \text{and} \quad \sigma_{t\theta} = F_{t\theta}/A_\theta \tag{6}$$

where A_θ is the area of the cut face (Fig. 3b). By calculating $\sigma_{n\theta}$ and $\sigma_{t\theta}$ for two mutually perpendicular cut faces, principal stress can be determined. The principal stress quantities at each node can be obtained from the characteristic polynomial (i.e., quadratic or cubic equation in 2-D or 3-D, respectively). In this study, a practical method for determining the polynomial roots is used [35]. The nodal stress tensor calculation is an integral part of the new approach discussed in the following section, whereas the intra-element stress vector is used to evaluate the numerical results discussed in Section 5.1.

4.2. Fictitious stress approach

We propose a discrete modeling of continua that avoids the spurious stress production described in Section 2. Considering a planar regular grid under general loading conditions (e.g., Fig. 4a), the following steps are taken:

Step 1. The lattice model is constructed and nodal displacements are determined for the case of $\alpha_1 = \alpha_2 = 1$ (Eq. (1)), which corresponds to $\nu = 0$. Principal stresses, σ_I, are calculated at each nodal site based on the nodal stress tensor calculations described in Section 4.1. Likewise, principal strains, ε_I, can be calculated. The index $I = 1$ or 2 for the direction of the major or minor principal stress/strain, respectively.

Step 2. We define a fictitious measure of orthogonal strain, by using the calculated principal strains and actual non-zero value of νaccording to:

$$\varepsilon_1' = \nu\varepsilon_2 \tag{7}$$

$$\varepsilon_2' = \nu\varepsilon_1 \tag{8}$$

Multiplying both sides by E, the fictitious stress can be calculated as:

$$\sigma_1' = \nu\sigma_2 \tag{9}$$

$$\sigma_2' = \nu\sigma_1 \tag{10}$$

Now, the fictitious force at a node (e.g., Fig. 4b) is

$$F_I' = \sigma_I' A_{\theta,I} \tag{11}$$

where A_θ is the area of the cut facet through the lattice node. The normal to $A_{\theta,I}$ is in direction I. This fictitious force is balanced by opposing forces acting on the cell facets (Fig. 4b). The magnitude of the force on each facet is proportional to the projected area of the facet on $A_{\theta,I}$. These fictitious forces are resolved into normal and tangential components and introduced into

the spring network. The set of fictitious forces associated with a given cell is self-equilibrating, as shown in Fig. 4c.

Step 3. Nodal displacements are calculated again, with the boundary conditions used in Step 1 and the fictitious spring forces obtained in Step 2. The new principal stresses, $\hat{\sigma_I}$, are calculated at each nodal site. The procedure ends if $||\hat{\sigma_I}-\sigma_I|| < e$, which is a predefined tolerance; otherwise Steps 2 and 3 are repeated with updated $\sigma_I=\hat{\sigma_I}$. With each iteration successively smaller increments of fictitious spring force are accumulated until the solution converges.

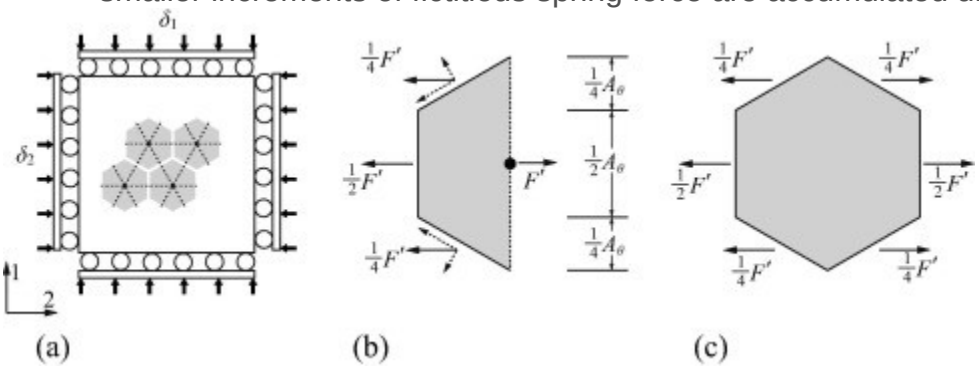

Download high-res image (125KB)

Download full-size image

Fig. 4. (a) Planar regular lattice under biaxial compression (showing nodal and elemental arrangements, along with associated hexagonal cells); (b) fictitious forces applied to a sectioned cell; and (c) fictitious forces acting on a complete cell.

For the special case of $\sigma_2 = 0$ with no lateral restraint, iteration is not required: $||\hat{\sigma_I}-\sigma_I|| \approx 0$. With such boundary conditions, the fictitious spring forces stretch the lattice network in the lateral direction, but do not change the stress field. This results from the proper distribution of the fictitious spring forces (Fig. 4b) based only on the fictitious stress at the lattice nodes (Eqs. (9), (10)). The contribution of this fictitious spring force to the network is analogous to uniform thermal expansion in a 1-D bar without restraint. Another special case in which iteration is not required is when both vertical and lateral boundaries are restrained as shown in Fig. 4a. For such boundary conditions, the fictitious stresses for each subsequent iteration $k = 2, 3,\ldots, n$, are

$$\sigma_1^{\prime(k)} = \nu\sigma_2^{\prime(k-1)} \tag{12}$$

$$\sigma_2^{\prime(k)} = \nu\sigma_1^{\prime(k-1)} \tag{13}$$

where $\sigma_1^{\prime(1)} = \nu\sigma_2$ and $\sigma_2^{\prime(1)} = \nu\sigma_1$. The cumulative effect of the iteration process can be expressed as:

$$\sigma_1' = \sum_{i=1}^{n} \sigma_1^{\prime(i)} \tag{14}$$

$$\sigma_2' = \sum_{i=1}^{n} \sigma_2^{\prime(i)} \tag{15}$$

Substituting Eqs. (12), (13) into Eqs. (14), (15), respectively, asymptotic values of the fictitious stresses can be obtained

$$\sigma_1' = \sigma_1 \sum_{i=1}^{\infty} \nu^{2i} + \sigma_2 \sum_{i=1}^{\infty} \nu^{2i-1} \tag{16}$$

$$\sigma_2' = \sigma_2 \sum_{i=1}^{\infty} \nu^{2i} + \sigma_1 \sum_{i=1}^{\infty} \nu^{2i-1} \tag{17}$$

For general boundary conditions, iteration is required over Steps 2 and 3. Convergence is expected, because the fictitious spring forces become smaller by a factor of ν, which is generally less than 0.5, for each successive iteration. Since the stiffness matrix remains the same for the displacement calculations in Steps 1 and 3, and any subsequent iterations, the computational expense of this approach is minor. For example, if the displacements are determined by Gaussian elimination in the first pass through Step 1, subsequent displacement calculations are made by the process of back substitution, using the factorized stiffness matrix and updated load vector. This approach is in some ways similar to that of Fang et al. [13], who iteratively introduce the Poisson effect into a rigid-body-spring lattice. This is done by adding a residual force vector, associated with the Poisson effect, into the right-hand side of the matrix equations that express global force equilibrium. Although the present discussion focuses on elastic response, the proposed procedure can be applied within fracture analyses. Hereafter, the accuracy of this fictitious stress approach is demonstrated in the following section.

5. Compression test simulation

Consider a rectangular domain with a quasi-circular inclusion (Fig. 5). Homogenous or heterogeneous systems are modeled by assigning the same set, or differing sets, of material properties for the inclusion and its surroundings. Uniform compressive strain is introduced by imposing a vertical displacement, δ, on the top platen, without lateral restraint.

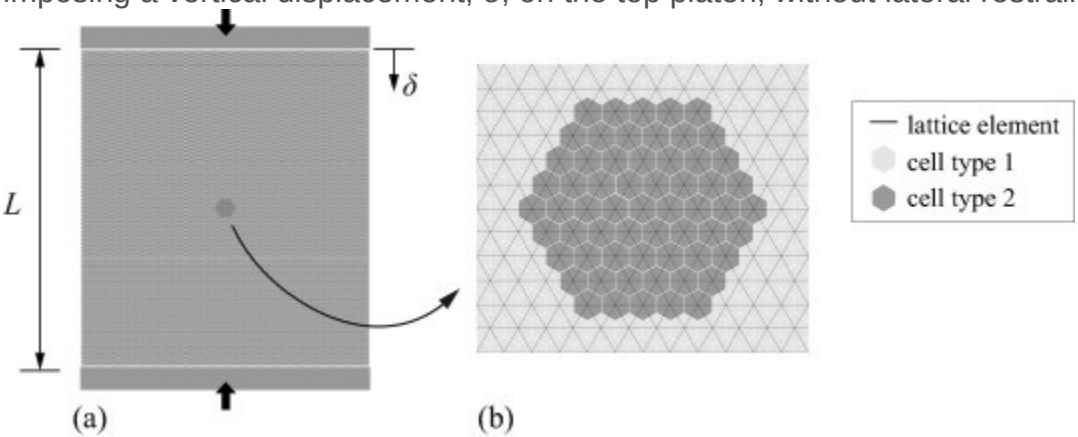

Download high-res image (424KB)

Download full-size image

Fig. 5. (a) Planar lattice with 19,547 nodes under compressive loading, and (b) enlarged view at the central area. The material properties of cell types 1 and 2 are same for the homogeneous system (Section 5.1), whereas they differ for the heterogeneous system (Section 5.2).

5.1. Homogeneous systems

In the following elastic analysis, results of the proposed approach for $\nu = 0.2$ and 0.4 are compared with results based on two different sets of spring constants: (i) $\alpha_1 = \alpha_2 = 1$ for $\nu = 0$; and (ii) $\alpha_1 = 1.25$ and $\alpha_2 = 1.25/3$ for macroscopic representation of $\nu = 0.2$ according to Eq. (2). The case of $\nu = 0.4$ is presented to demonstrate capabilities of the approach for Poisson ratios outside the range accommodated by ordinary lattice models. Comparisons are made in terms of nodal displacement, nodal stress, and elemental stress. The results presented in this section are based on a single sequence of the fictitious stress approach without iteration. Table 1 presents the average values and standard deviations of the computed displacement, u_h, which has been normalized by the exact value, u. All results presented in the table agree reasonably well with theory. Notably, regular lattices based on the fictitious stress approach accurately represent the Poisson effect beyond the upper limit of $\nu = 1/3$ for ordinary lattice models.

Table 1. Average values, μ, and standard deviations, σ_{std}, of normalized displacements, u_h/u, for uniaxial compression loading.

Poisson ratio, ν		**0.0**	**0.2**	**0.2**	**0.4**
Coefficients of Eq. (1)		$\alpha_1 = \alpha_2 = 1$	$\alpha_1 = 1.25$, $\alpha_2 = 1.25/3$	$\alpha_1 = \alpha_2 = 1$	$\alpha_1 = \alpha_2 = 1$
Fictitious stresses introduced		No	No	Yes	Yes
Loading direction values	μ	1.0000	0.9999	0.9999 (1.0000)[a]	0.9998 (1.0000)[a]
	σ_{std}	3.21×10^{-10}	2.75×10^{-4}	1.25×10^{-4} (1.91×10^{-8})[a]	2.49×10^{-4} (8.80×10^{-8})[a]
Lateral direction values	μ	–	1.0001	1.0002 (1.0000)[a]	1.0002 (1.0000)[a]
	σ_{std}	–	2.00×10^{-3}	3.01×10^{-3} (6.06×10^{-6})[a]	3.01×10^{-3} (6.03×10^{-6})[a]

[a] Values in parentheses are based on correct application of the fictitious stresses on the elements framing into boundary nodes.

The current implementation of the stress calculations (Section 4.1) does not account for the lack of elements associated with boundary facets. The stress values along the boundaries are therefore inaccurate, which degrades the accuracy of the fictitious stress approach. If the fictitious stresses are correctly applied to the elements connected to the boundary nodes, the overall accuracy is improved as shown by the values in parentheses in Table 1.

Fig. 6 shows the Mohr circle representation of stress at each of the internal nodes, as provided by the nodal stress tensor calculations for $\theta = n\pi$ where $n = 0$ to 2 with an interval of 1/18. Each of the dots

represents the stress pair ($\sigma_{n\theta}$ and $\sigma_{t\theta}$ in Eq. (6)) results for each node for a particular inclination of the cut plane, θ. For the case of $\alpha_1 = \alpha_2 = 1$, including applications of the fictitious stress approach, Mohr's circle of stress is accurately produced at all internal nodes. Here, too, the ability to model cases where $\nu > 1/3$ is demonstrated. On the other hand, discrepancies with the theoretical results arise for the case of macroscopic representation of $\nu = 0.2$ by assigning $\alpha_1 = 1.25$ and $\alpha_2 = 1.25/3$. In particular, the major principal stress at each node is non-zero.

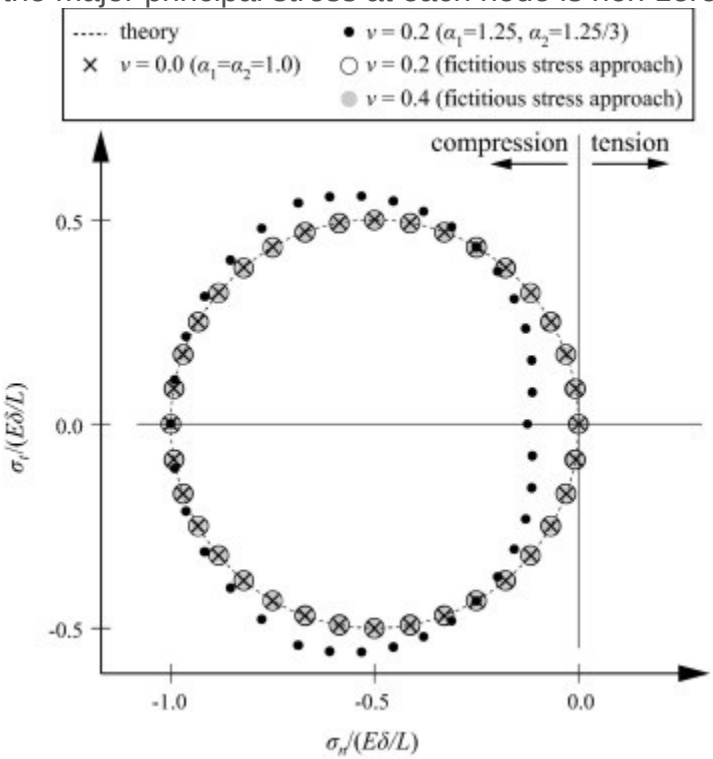

Download high-res image (176KB)

Download full-size image

Fig. 6. Mohr's circle representation of nodal stress state under uniaxial compressive loading.

Fig. 7 shows the vectorial stress pair results, obtained by Eq. (3), for all elements in the domain. The number of distinct stress values appearing in Fig. 7 is small, since a regular mesh has been used to discretize a homogeneous material under uniform loading. Here too, the local stress representation of the fictitious stress approach agrees well with theory, whereas errors occur for the case where $\nu = 0.2$ ($\alpha_1 = 1.25$ and $\alpha_2 = 1.25/3$). For this case, the lateral elements exhibit tensile stress, which does not appear in an elastic continuum under the same loading pattern, as discussed in Section 2. Such a discrepancy would strongly and incorrectly influence the modeling of fracture based on elemental stresses.

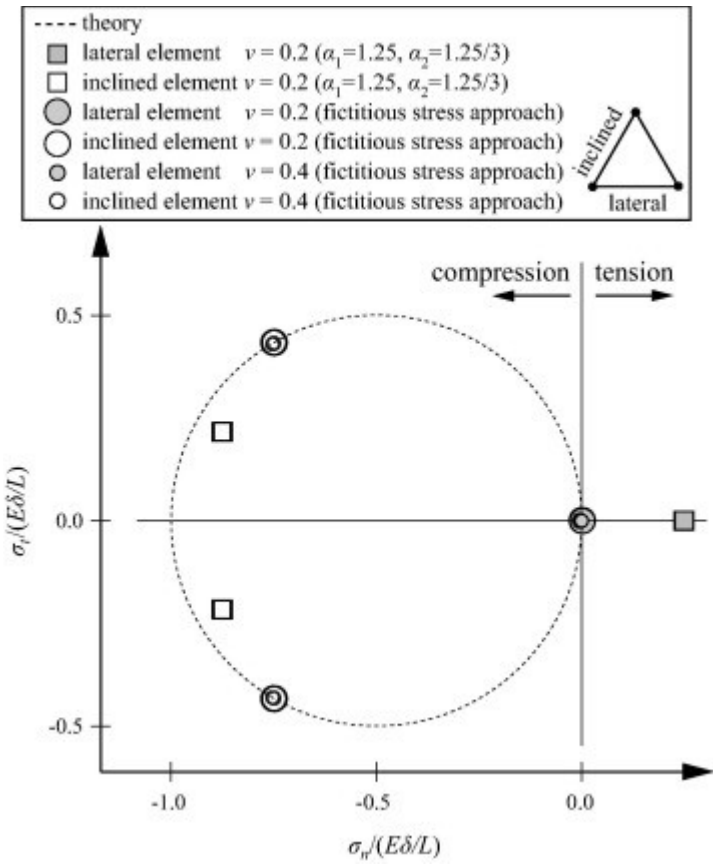

Download high-res image (244KB)

Download full-size image

Fig. 7. Elemental stress states for a homogeneous material under uniaxial compressive loading.

The needs to remedy inadequacies in representing the Poisson effect are even greater when using irregular lattices [3]. The large amount of scatter, which is due to irregular geometry of the lattice, cannot be removed by calibration of the spring coefficients. Such form of artificial heterogeneity is undesirable in that it does not correspond to physical features of the material. We anticipate implementing the fictitious stress approach within irregular lattice models for general stress analyses of elastic materials. The same steps outlined in Section 4.2 are retained. The main difference is in the calculation of fictitious forces assigned to each facet (Fig. 4b), which is more involved for irregular polygonal cells. Future developments are necessary to extend the approach to irregular and three-dimensional lattices.

5.2. Heterogeneous systems

The same 2-D domain and boundary conditions used in the previous example are employed, except a stiffer inclusion is centrally installed within the domain (Fig. 5). The inclusion and matrix phase have a modular ratio $E_i/E_m = 3$, whereas the Poisson ratio is assumed to be the same for both phases. Here, two cases are considered: $\nu = 0$, and $\nu = 0.2$, for which the corresponding contour diagrams of principal tensile stress are shown in Fig. 8, Fig. 9, respectively. In both figures, the normalizing factor is $\sigma = E_m\delta/L$. Each figure also presents results based on constant strain triangle (CST) finite elements. For objective comparisons, the finite element (FE) discretization is based on the same Delaunay

tessellation that defines the lattice topology (Fig. 5). For the fictitious stress approach, three iterations are required to satisfy the convergence criterion defined in step 3 of Section 4.2, where tolerance e was set in accordance with the level of accuracy of the nodal stress calculations. Only the right half of the domain is shown due to the symmetry of the domain and boundary conditions.

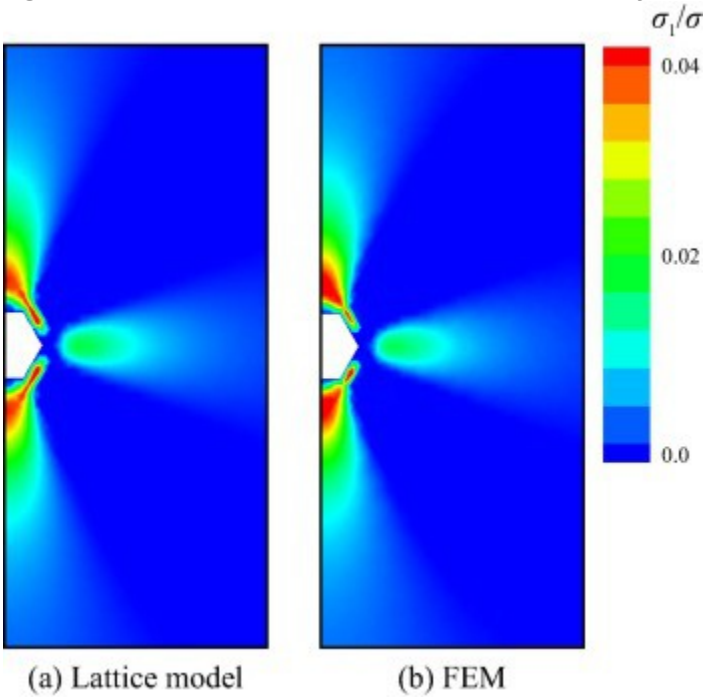

Download high-res image (125KB)

Download full-size image

Fig. 8. Principal tensile stress local to a stiff circular inclusion within a rectangular domain under applied compressive strain, for $\nu = 0$: (a) lattice model with $\alpha_1 = \alpha_2 = 1$, and (b) finite element method (FEM).

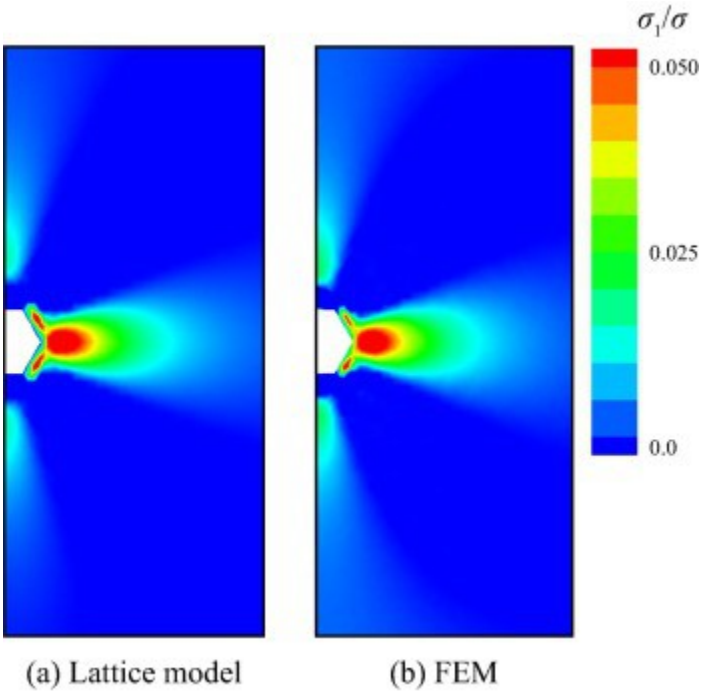

Download high-res image (119KB)

Download full-size image

Fig. 9. Principal tensile stress local to a stiff circular inclusion within a rectangular domain under applied compressive strain, for $\nu = 0.2$: (a) lattice model using the fictitious stress approach, and (b) finite element method (FEM).

For the case with $\nu = 0$ (Fig. 8), the lattice results and FE results agree well and exhibit higher tensile stresses above and below the inclusion. For the case with $\nu = 0.2$ (Fig. 9) as well, the results from both approaches agree well. However, the region of highest tensile stress appears to the side of the inclusion. Accuracy of the proposed approach is further demonstrated in Fig. 10, which compares principal tensile stress values along vertical and horizontal lines from the inclusion boundary for the cases of $\nu = 0$ and $\nu = 0.2$, respectively. Differences between the lattice and FE results are partly due to the averaging of finite element stresses to obtain nodal values, from which the contours have been drawn. Representation of the inclusion boundary differs depending on whether lattice or triangular finite elements are used, which also contributes to differences in the stress values.

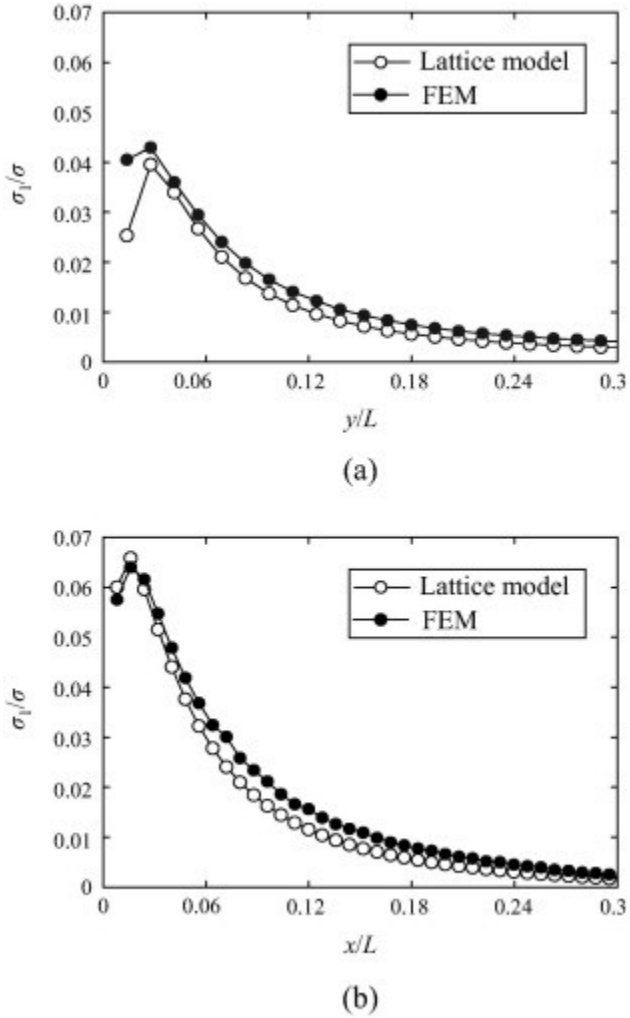

Download high-res image (208KB)

Download full-size image

Fig. 10. Principal tensile stress along: (a) a vertical line originating from the upper boundary of the inclusion for $\nu = 0$; and (b) a horizontal line originating from the right boundary of the inclusion for $\nu = 0.2$.

It is clear that the Poisson effect can greatly influence the stress conditions within heterogeneous systems even when the Poisson ratio of each phase is the same. Similar results have been achieved by coupling lattice models with triangular finite elements [6]. Whereas their results require the use of continuum finite elements, the approach proposed herein involves only two-node lattice elements, which facilitates the modeling of some aspects of fracture. Classical lattice models represent fracture as an event-by-event process, in which each event (i.e., the breaking of a single lattice element) is preceded by a linear elastic solution of the equilibrium equations [17]. As a next step, we anticipate conducting the fictitious stress approach within each solution cycle, such that the Poisson effect is represented within stress values utilized by the fracture criteria.

6. Conclusion

Due to the two-node element representation of the displacement field, ordinary lattice models do not properly simulate local stress conditions for general elastic media (i.e., for arbitrary choices of E and ν within appropriate limits). Direct relationships between the macroscopic elastic constants and the spring constants have been sought. Such relationships may satisfy strain conditions for regular lattices. As shown herein, however, the local stress conditions are not satisfied even for regular lattices. For irregular lattices, stress values not only differ from theory, but also exhibit a large scatter. Such discrepancies complicate the modeling of fracture with stress-based criteria.
The approach presented herein remedies the inabilities of regular lattice models to calculate local measures of stress. Based on tensorial representations of stress at each node, a set of fictitious forces are calculated and introduced into the lattice in a manner that correctly produces the Poisson effect. The stiffnesses of the lattice elements are defined by the elastic constants (E, ν) without any need for calibration with laboratory test results. The examples provided herein demonstrate both global strain and local stress representations are correctly captured for arbitrary Poisson ratio. Previous restrictions on the upper limit of ν for regular planar lattices are overcome, as demonstrated by results for $\nu \geqslant 1/3$ in this paper. Future developments are necessary to extend the approach to irregular and three-dimensional lattices.

References

[1]
M.D. Adley, M.H. Sadd**Continuum models for materials with lattice-like microstructure**
Comput Struct, 43 (1) (1992), pp. 13-18
ArticleDownload PDFView Record in Scopus
[2]
D. Asahina, J.E. Houseworth, J.T. Birkholzer, J. Rutqvist, J.E. Bolander**Hydro-mechanical model for wetting/drying and fracture development in geomaterials**
Comput Geosci, 65 (2014), pp. 13-23
ArticleDownload PDFView Record in Scopus
[3]
D. Asahina, E.N. Landis, J.E. Bolander**Modeling of phase interfaces during pre-critical crack growth in concrete**
Cem Concr Compos, 33 (9) (2011), pp. 966-977

ArticleDownload PDFView Record in Scopus
[4]
Z.P. Bažant, M.R. Tabbara, M.T. Kazemi, G. Pyaudier-Cabot**Random particle model for fracture of aggregate or fiber composites**
J Eng Mech, 116 (8) (1990), pp. 1686-1705
CrossRefView Record in Scopus
[5]
E. Benvenuti, A. Tralli, G. Ventura**A regularized XFEM model for the transition from continuous to discontinuous displacements**
Int J Numer Methods Eng, 74 (6) (2008), pp. 911-944
CrossRefView Record in Scopus
[6]
Bolander JE, Moriizumi K, Kunieda M, Yip M. Rigid-body-spring network modeling of cement-based composites. In: The 4th international conference on fracture mechanics of concrete and concrete structures (FraMCoS-4); 2001. p. 773–80.
[7]
J.E. Bolander, S. Saito**Fracture analyses using spring networks with random geometry**
Eng Fract Mech, 61 (5–6) (1998), pp. 569-591
ArticleDownload PDFView Record in Scopus
[8]
B. Chiaia, A. Vervuurt, J.G.M. Van Mier**Lattice model evaluation of progressive failure in disordered particle composites**
Eng Fract Mech, 57 (1997), pp. 301-318
ArticleDownload PDFView Record in Scopus
[9]
Cundall PA. A computer model for simulating progressive large scale movements in blocky rock systems. In: Proceedings of the symposium of the international society rock mechanics; 1971.
[10]
G. Cusatis, Z.P. Bažant, L. Cedolin**Confinement-shear lattice model for concrete damage in tension and compression: I. theory**
J Eng Mech, 129 (12) (2003), pp. 1439-1448
CrossRefView Record in Scopus
[11]
G. Cusatis, D. Pelessone, A. Mencarelli**Lattice discrete particle model (LDPM) for failure behavior of concrete. I: Theory**
Cem Concr Compos, 33 (9) (2011), pp. 881-890
ArticleDownload PDFView Record in Scopus
[12]
Cusatis G, Schauffert EA. Discontinuous cell method (DCM) for cohesive fracture propagation. In: The 7th international conference on fracture mechanics of concrete and concrete structures (FraMCoS-7); 2010. p. 529–35.
[13]
Y. Fang, B.N. Nguyen, K. Carroll, Z. Xu, S.B. Yabusaki, T.D. Scheibe, *et al.***Development of a coupled thermo-hydro-mechanical model in discontinuous media for carbon sequestration**
Int J Rock Mech Min Sci, 62 (2013), pp. 138-147

ArticleDownload PDFView Record in Scopus
[14]
H. Gercek**Poisson's ratio values for rocks**
Int J Rock Mech Min Sci, 44 (1) (2007), pp. 1-13
ArticleDownload PDFView Record in Scopus
[15]
P. Grassl, C. Fahy, D. Gallipoli, S.J. Wheeler**On a 2D hydro-mechanical lattice approach for modelling hydraulic fracture**
J Mech Phys Solids, 75 (2015), pp. 104-118
ArticleDownload PDFView Record in Scopus
[16]
D.V. Griffiths, G.G.W. Mustoe**Modelling of elastic continua using a grillage of structural elements based on discrete element concepts**
Int J Numer Methods Eng, 50 (7) (2001), pp. 1759-1775
CrossRefView Record in Scopus
[17]
H. Herrmann, S. Roux**Statistical models for the fracture of disordered media**
North Holland, Amsterdam, The Netherlands (1990)
[18]
M. Hori, K. Oguni, H. Sakaguchi**Proposal of FEM implemented with particle discretization for analysis of failure phenomena**
J Mech Phys Solids, 53 (3) (2005), pp. 681-703
ArticleDownload PDFView Record in Scopus
[19]
A. Hrennikoff**Solution of problems of elasticity by the framework method**
J Appl Mech, 8 (4) (1941), pp. 169-175
[20]
A. Jagota, S.J. Bennison**Spring-network and finite-element models for elasticity and fracture**
K. Bardhan, B. Chakrabarti, A. Hansen (Eds.), Non-linearity and breakdown in soft condensed matter, vol. 437, Springer, Berlin Heidelberg (1994), pp. 186-201
CrossRefView Record in Scopus
[21]
L. Jing**A review of techniques, advances and outstanding issues in numerical modelling for rock mechanics and rock engineering**
Int J Rock Mech Min Sci, 40 (3) (2003), pp. 283-353
ArticleDownload PDFView Record in Scopus
[22]
R. Katsman, E. Aharonov, H. Scher**Numerical simulation of compaction bands in high-porosity sedimentary rock**
Mech Mater, 37 (1) (2005), pp. 143-162
ArticleDownload PDFView Record in Scopus
[23]
T. Kawai**New discrete models and their application to seismic response analysis of structures**
Nucl Eng Des, 48 (1) (1978), pp. 207-229

ArticleDownload PDFView Record in Scopus
[24]
A. Lisjak, G. Grasselli, T. Vietor**Continuum–discontinuum analysis of failure mechanisms around unsupported circular excavations in anisotropic clay shales**
Int J Rock Mech Min Sci, 65 (2014), pp. 96-115
ArticleDownload PDFView Record in Scopus
[25]
C. Liu, D.D. Pollard, B. Shi**Analytical solutions and numerical tests of elastic and failure behaviors of close-packed lattice for brittle rocks and crystals**
J Geophys Res: Solid Earth, 118 (1) (2013), pp. 71-82
CrossRefView Record in Scopus
[26]
O.K. Mahabadi, A. Lisjak, A. Munjiza, G. Grasselli**Y-Geo: new combined finite–discrete element numerical code for geomechanical applications**
Int J Geomech, ASCE, 12 (6) (2012), pp. 676-688
CrossRefView Record in Scopus
[27]
A. Munjiza**The combined finite–discrete element method**
John Wiley & Sons Ltd., Chichester, West Sussex, England (2004)
[28]
A. Munjiza, E.E. Knight, E. Rougier**Computational mechanics of discontinua**
John Wiley & Sons Ltd. (2012)
[29]
J. Oliver, A. Huespe, M. Pulido, E. Chaves**From continuum mechanics to fracture mechanics: the strong discontinuity approach**
Eng Fract Mech, 69 (2) (2002), pp. 113-136
ArticleDownload PDFView Record in Scopus
[30]
P.-Z. Pan, F. Yan, X.-T. Feng**Modeling the cracking process of rocks from continuity to discontinuity using a cellular automaton**
Comput Geosci, 42 (2012), pp. 87-99
ArticleDownload PDFView Record in Scopus
[31]
D.O. Potyondy, P.A. Cundall**A bonded-particle model for rock**
Int J Rock Mech Min Sci, 41 (8) (2004), pp. 1329-1364
ArticleDownload PDFView Record in Scopus
[32]
E. Schlangen, E.J. Garboczi**Fracture simulations of concrete using lattice models: computational aspects**
Eng Fract Mech, 57 (2–3) (1997), pp. 319-332
ArticleDownload PDFView Record in Scopus
[33]
E. Schlangen, J.G.M. Van Mier**Experimental and numerical analysis of micromechanisms of fracture of cement-based composites**

Cem Concr Compos, 14 (1992), pp. 105-118
ArticleDownload PDFView Record in Scopus
[34]
E. Tamayo-Mas, A. Rodríguez-Ferran**A new continuous-discontinuous damage model: cohesive cracks via an accurate energy-transfer process**
Theor Appl Fract Mec, 69 (2014), pp. 90-101
ArticleDownload PDFView Record in Scopus
[35]
A.C. Ugural, S.K. Fenster**Advanced strength and applied elasticity**
Prentice Hall (2003)
[36]
C. Yao, Q.H. Jiang, J.F. Shao**Numerical simulation of damage and failure in brittle rocks using a modified rigid block spring method**
Comput Geotech, 64 (2015), pp. 48-60
ArticleDownload PDFView Record in Scopus
[37]
M. Yip, J. Mohle, J.E. Bolander**Automated modeling of three-dimensional structural components using irregular lattices**
Comput-Aided Civ Infrastruct Eng, 20 (2005), pp. 393-407
CrossRefView Record in Scopus
[38]
J. Yoon**Application of experimental design and optimization to PFC model calibration in uniaxial compression simulation**
Int J Rock Mech Min Sci, 44 (6) (2007), pp. 871-889
ArticleDownload PDFView Record in Scopus